Dual-plane miniature planar 3D ECT sensor based on 3 × 3 matrix electrode array

Wen Pin Gooi and Pei Ling Leow
Faculty of Electrical Engineering, Universiti Teknologi Malaysia, Skudai, Malaysia
Jaysuman Pusppanathan
Sport Innovation and Technology Centre (SiTC), Institute of Human Centered Engineering (iHumen), Universiti Teknologi Malaysia, Skudai, Malaysia, and
Xian Feng Hor and Shahrulnizahani Mohammad Din
Faculty of Electrical Engineering, Universiti Teknologi Malaysia, Skudai, Malaysia

Abstract

Purpose – As one of the tomographic imaging techniques, electrical capacitance tomography (ECT) is widely used in many industrial applications. While most ECT sensors have electrodes placed around a cylindrical chamber, the planar ECT sensor has been investigated for depth and defect detection. However, the planar ECT sensor has limited height and depth sensing capability due to its single-sided assessment with the use of only a single-plane design. The purpose of this paper is to investigate a dual-plane miniature planar 3D ECT sensor design using the 3 × 3 matrix electrode array.

Design/methodology/approach – The sensitivity map of dual-plane miniature planar 3D ECT sensor was analysed using 3D visualisation, the singular value decomposition and the axial resolution analysis. Then, the sensor was fabricated for performance analysis based on 3D imaging experiments.

Findings – The sensitivity map analysis showed that the dual-plane miniature planar 3D ECT sensor has enhanced the height sensing capability, and it is less ill-posed in 3D image reconstruction. The dual-plane miniature planar 3D ECT sensor showed a 28% improvement in reconstructed 3D image quality as compared to the single-plane sensor set-up.

Originality/value – The 3 × 3 matrix electrode array has been proposed to use only the necessary electrode pair combinations for image reconstruction. Besides, the increase in number of electrodes from the dual-plane sensor setup improved the height reconstruction of the test sample.

Keywords Sensors, Capacitive, Electrical tomography

Paper type Research paper

Introduction

Electrical capacitance tomography (ECT) is a non-invasive electrical tomography technique that is widely used in industrial application such as fluidised bed (Porzuczek, 2014; Huang *et al.*, 2019; Wang and Yang, 2021) and multiphase flow measurement (Yao and Takei, 2017; Rodriguez-Frias and Yang, 2020; Ye *et al.*, 2020; Shen *et al.*, 2021). The ECT reconstructs images based on the permittivity distribution by mapping the changes in interelectrode capacitance to the sensitivity distribution. While the typical ECT sensor has electrodes placed around a pipeline, another variant of the ECT sensor based on the planar electrode configuration also exists. The planar ECT sensor has electrodes distributed uniformly on an electrode plane and uses the fringing electric field for detection of objects. A lot of effort has been put into the research of planar ECT sensor for applications such as landmine scanning (Tholin-Chittenden and Soleimani, 2017; Tholin-Chittenden *et al.*, 2018), surface or subsurface defect detection (Wen *et al.*, 2017; Pan *et al.*, 2021; Suo *et al.*, 2021; Zhang *et al.*, 2021) and obstacle and pressure sensing in robotics (Ma and Soleimani, 2020). Although the single-plane planar ECT sensor is reported to successfully reconstruct 2D or 3D images and locate the position of defects correctly, it has limitation in terms of the height sensing and depth detection. This is due to the single-sided assess of single-plane planar ECT sensor which has decreasing sensitivity as the distance from the sensor surface increases.

To address the shortcomings of single-plane planar ECT sensors, the multiple planes planar ECT sensor has been investigated. Ye *et al.* (2015) studied the effect of reducing the electrode planes on the quality of reconstructed image using a six planes 3D ECT sensor with four electrodes on each plane. The experimental results showed that the 3D image quality deteriorated with the reduction of electrode planes, and a minimum of two electrode planes were needed to produce reasonable quality 3D image. Wei *et al.* (2015) compared the performance of single- and dual-plane 3D ECT sensor. Despite the reported improvement in 3D image reconstruction using the dual-plane 3D ECT sensor, the frame rate was reduced due to the increase in number of electrodes from 12 to 24. Towards the miniaturisation of multiple planes planar ECT sensor, Ren and Yang (2015, 2017) reported on a flexible design of

The current issue and full text archive of this journal is available on Emerald Insight at: **https://www.emerald.com/insight/0260-2288.htm**

Sensor Review
43/5/6 (2023) 369–378

[DOI 10.1108/SR-06-2023-0240]

This study was supported by Ministry of Higher Education Malaysia and Universiti Teknologi Malaysia through FRGS project code: FRGS/1/2020/TK0/UTM/02/47.

Received 29 June 2023
Revised 26 August 2023
Accepted 26 August 2023

dual-plane ECT sensor using 2 × 3 electrode array on each plane. The ECT sensor successfully reconstructed the 2D image of tooth surface with satisfactory quality and suggested that increasing the number of electrodes can further improve the image quality. Hor *et al.* (2023) optimised the design of miniature dual-plane 3D ECT sensor using the planar peripheral electrodes for the integration onto on-chip platform. The experimental results showed that the 3D image of yeast encapsulated in agar can be reconstructed, but the image quality and the height reconstruction of test samples were highly dependent on the location in the sensing region.

The number of electrodes in the reported dual-plane ECT sensors is either insufficient or too much, and the image quality is dependent on the electrode placement in the sensing region. Thus, this paper investigates a dual-plane miniature planar 3D ECT sensor using nine distributed electrodes arranged in 3 × 3 matrix electrode array in each electrode plane. The proposed 3 × 3 matrix electrode array optimises the electrode pairs to neighbouring and opposing electrode pairs only, as these electrode pairs contribute the most to image reconstruction (Wen *et al.*, 2017). The sensitivity distribution of dual-plane on-chip 3D ECT sensor was analysed and compared to the single-plane miniature planar 3D ECT sensor for studying its feasibility in improving the height of 3D reconstructed image. Then, the dual- and single-plane miniature planar 3D ECT sensors were fabricated and characterised experimentally in terms of the optimal sensing height and the capacitance measurement. In addition, the improvement in height reconstruction of dual-plane miniature planar 3D ECT sensor was evaluated and compared to the single-plane miniature planar 3D ECT sensor based on the quantitative analysis of the reconstructed 3D image.

Principle of electrical capacitance tomography

The computation of the permittivity distribution in ECT involves two processes which are the forward and inverse problems. The forward problem models the 3 × 3 matrix electrode array dual-plane miniature planar 3D ECT sensor and the sensing region to obtain a relationship between the capacitance measurement and the permittivity distribution. The forward problem relationship of capacitance and permittivity distribution is given by:

$$\mathrm{C} = \frac{1}{\mathrm{V}} \iiint \varepsilon(\mathrm{x},\mathrm{y},\mathrm{z})\mathrm{E}(\mathrm{x},\mathrm{y},\mathrm{z})\mathrm{dx}\,\mathrm{dy}\,\mathrm{dz} \tag{1}$$

where C is the interelectrode capacitance, $\varepsilon(x,y,z)$ is the permittivity distribution, $E(x,y,z)$ is the electric field distribution and V is the potential difference between the excitation and sensing electrodes. To simplify the computation of permittivity distribution, (1) can be linearised as:

$$\mathrm{C} = \mathrm{S}\varepsilon \tag{2}$$

where S is the sensitivity map that relates the degree of changes in permittivity distribution to the changes in interelectrode capacitance. Based on (2), the permittivity distribution can be computed by solving the equation as an inverse problem, given the sensitivity map and the interelectrode capacitance measurements. The sensitivity map between ith and jth electrode pair is expressed as:

$$\mathrm{S_{ij}}(\mathrm{x},\mathrm{y},\mathrm{z}) = -\int_{\vartheta(\mathrm{x},\mathrm{y},\mathrm{z})} \frac{\mathrm{E_i}(\mathrm{x},\mathrm{y},\mathrm{z})}{\mathrm{V_i}} \cdot \frac{\mathrm{E_j}(\mathrm{x},\mathrm{y},\mathrm{z})}{\mathrm{V_j}} d\vartheta \tag{3}$$

where $S_{ij}(x,y,z)$ is the sensitivity map for ith and jth electrode pair. There are a total of 153 sensitivity maps because the 18 electrodes of dual-plane miniature planar 3D ECT sensor has 153 possible electrode pair combinations. The sensitivity maps are arranged in the form of $M \times N$ matrix, where M is the electrode pair combinations and N is the number of voxels. $E_i(x,y,z)$ and $E_j(x,y,z)$ are the electric field distribution when ith and jth electrodes are supplied with excitation voltage V_i and V_j, respectively, while the remaining electrodes are grounded.

In this study, the linear back projection (LBP) algorithm is used to solve the inverse problem for image reconstruction. In LBP, the transpose of S, $\mathrm{S^T}$, is used because the inverse of S does not exist. The normalised form of LBP algorithm is given by:

$$\varepsilon = \frac{\mathrm{S^T C}}{\mathrm{S^T u_C}} \qquad \mathrm{u_C} = [1, 1, \ldots, 1] \tag{4}$$

where $\mathrm{u_C}$ is an identity vector. The LBP algorithm is chosen due to its simplicity, fast imaging speed and it is widely used (Ren and Yang, 2015; Yang *et al.*, 2017). Because LBP is a basic algorithm, the performance of dual-plane on-chip 3D ECT sensor can be evaluated with minimal interference from image reconstruction algorithm.

Simulation study

Dual-plane miniature planar 3D electrical capacitance tomography sensor model

Figure 1 shows the 3D simulation model of dual-plane miniature planar 3D ECT sensor. The sensor consists of a top and a bottom electrode plane. Each electrode plane consists of nine square electrodes that are arranged in a 3 × 3 matrix array. Because two electrode planes are used, the sensor has a total of 18 electrodes. The electrodes E1 to E9 made up the bottom electrode plane, while electrodes E10 to E18 made up the top electrode plane. The square electrode has a width of 3 mm, and the separation between each electrode is 1 mm. The 3 × 3 matrix electrode array is fitted into a cylindrical sensing chamber with a diameter of 17 mm and a height of 3 mm. The height of the sensing chamber was set to 3 mm, considering that the diameter of the sensing chamber in Yang *et al.*'s (2017) study was close to 17 mm that was used in this research. Moreover, the sensitive region reached half of the 3 mm height sensing chamber only in Yang *et al.*'s (2017) study.

The sensor model was simulated in COMSOL Multiphysics using the electrostatic module to compute the distribution of electric field in the sensing chamber for the computation of sensitivity map. The electric field distribution was simulated by exciting the excitation electrode with 1 V potential, and the remaining electrodes were set to ground potential. This process continued until all the electrodes were used as the excitation electrode once. A fine mesh was used in the simulation of electric field distribution. In this study, the sensing chamber was discretised into 64 × 64 × 10 voxels for 3D image reconstruction. Thus, the simulated electric field distribution was discretised based on the number of voxels and exported to MATLAB for the sensitivity map computation using (3) and analysis.

As a proof of concept that the miniature planar 3D ECT sensor with 3 × 3 matrix electrode array could reconstruct 3D image with comparable quality as the planar 3D ECT sensor

Figure 1 Simulation model of dual plane on-chip 3D ECT sensor

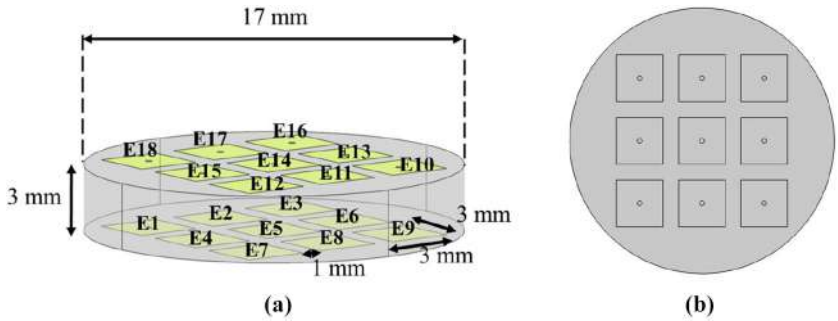

Notes: (a) Isometric view and (b) top view
Source: Figure by authors

with higher number of electrodes, a simulation image reconstruction was performed using the single-plane sensor setup of 3×3 and 4×4 matrix electrode arrays as shown in Figure 2. The square electrode of dimension in Figure 1 was used in this comparative study. A 2 mm cube phantom was simulated on electrode E5 and E6 of the 3×3 and 4×4 matrix single-plane miniature planar 3D ECT sensor, respectively. These locations are surrounded by the same number of neighbouring and opposing electrode pairs. The neighbouring and opposing electrode pair combinations comprise of combinations such as E1–E2 and E1–E5, respectively, as illustrated in Figure 1.

The simulation 3D image reconstruction results revealed that having more than nine electrodes does not improve the image quality drastically because the reconstructed 3D image of both sensors appeared identical. This shows that the 3D image reconstruction is primarily contributed by the neighbouring and opposing electrode pair combinations rather than all the electrode pair combinations available. Therefore, the proposed 3×3 matrix electrode array design in this study is practical, as it provides sufficient data for image reconstruction. In the following sections, the simulation analysis and experimental studies of dual-plane miniature planar 3D ECT sensor were conducted based on the 3×3 matrix electrode array.

Sensitivity map analysis

In this section, the sensitivity map of dual-plane miniature planar 3D ECT sensor was analysed based on visual inspection, singular value decomposition (SVD) analysis and axial resolution analysis. Figure 3 compares the 3D sensitivity map of the dual- and single-plane miniature planar 3D ECT sensors. The 3D sensitivity map was generated by plotting the isosurface of the average sum of sensitivity maps of all the electrode pair combinations.

As shown in Figure 3, the sensitive region of dual-plane miniature planar 3D ECT sensor extends from the bottom to the top of sensing chamber, whereas the sensitive region of single-plane miniature planar 3D ECT sensor reaches half of the sensing chamber only. The extended coverage of sensitive region is attributed to the sensitivity maps generated from

Figure 2 Single-plane ECT sensor model of (a) 3×3 matrix electrode array, (b) 4×4 matrix electrode array, (c) reconstructed 3D image of 3×3 matrix electrode array and (d) reconstructed 3D image of 4×4 matrix electrode array

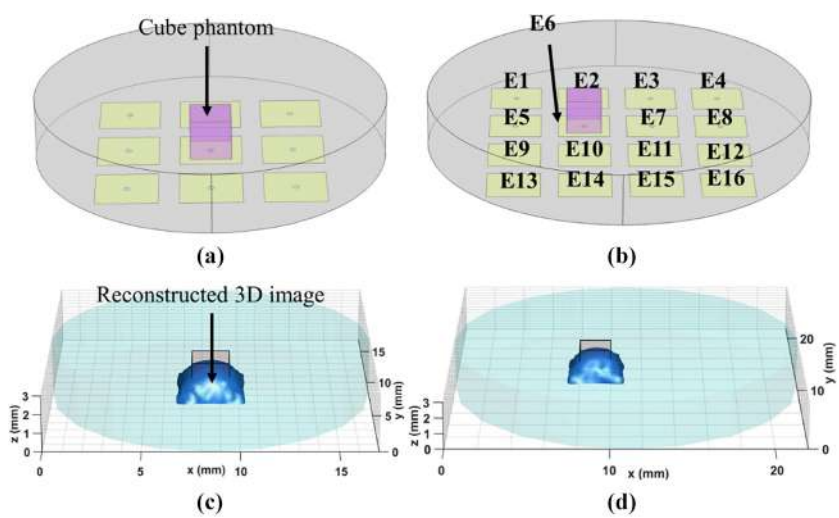

Source: Figure by authors

Figure 3 3D visualisation of sensitivity distribution of miniature planar 3D ECT sensors

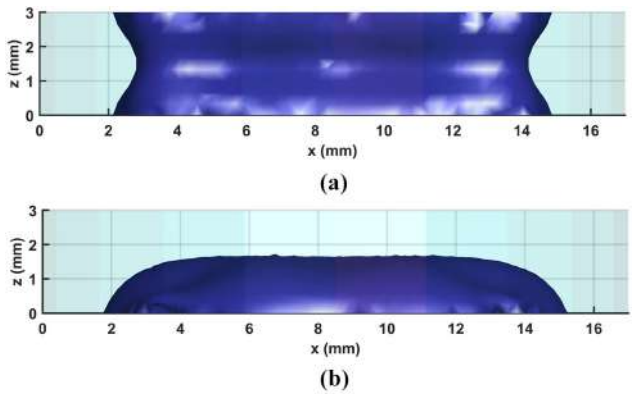

Notes: (a) dual-plane and (b) single-plane
Source: Figure by authors

electrode pair combinations between the bottom and top electrode planes and within the top plane itself. This indicates that the dual-plane miniature planar 3D ECT sensor could improve 3D image quality by enhancing the height reconstruction due to the presence of sensitivity coverage along the vertical direction. Meanwhile, the SVD analysis is performed to study the ill-posed condition and theoretical performance of the dual-plane miniature planar 3D ECT sensor in 3D image reconstruction. Figure 4 compares the normalised singular values of the dual- and single-plane miniature planar 3D ECT sensors.

As shown in Figure 4, the slope of single-plane miniature planar 3D ECT sensor is steeper than dual-plane miniature planar 3D ECT sensor. This indicates that the dual-plane miniature planar 3D ECT sensor is less ill-posed than single-plane miniature planar 3D ECT sensor in solving the inverse problem for image reconstruction. A high number of singular values above the noise level in SVD plot provide more useful projections that could improve the reconstructed image quality (Tholin-Chittenden and Soleimani, 2017). By assuming a noise level of 1% in capacitance measurement, the dual-plane miniature planar 3D ECT sensor has 73 singular values above noise level as compared to the 33 singular values of single-plane miniature planar 3D ECT sensor. This shows that the addition of top electrode plane in dual-plane miniature planar 3D ECT sensor increases the number of useful projections for image reconstruction, and the 3D imaging capability could outperform the single-plane miniature planar 3D ECT sensor. Nonetheless, the magnitude of singular values above the 1% noise level for dual-plane miniature planar 3D ECT sensor is larger than the single-plane miniature planar 3D ECT sensor, suggesting that the reconstructed 3D image is less affected by noise.

Figure 4 Normalised singular value comparison of dual- and single-plane miniature planar 3D ECT sensors above 1% noise threshold

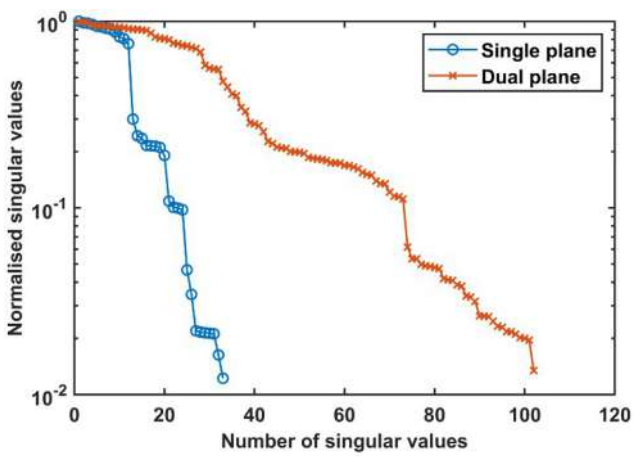

Source: Figure by authors

The axial resolution analysis is conducted to evaluate the variation in sensitivity distribution of dual-plane miniature planar 3D ECT sensor. The presence of sensitivity variation along the vertical direction reflects the ability of the dual-plane miniature planar 3D ECT sensor in reconstructing the height of imaging samples at specific test positions in the sensing chamber. Figure 5 compares the normalised sensitivity magnitude at different height in sensing chamber of dual- and single-plane miniature planar 3D ECT sensors. The test positions P1, P2, P3 and P4 where the axial resolution data are extracted are included in Figure 5 for reference. The test positions P1, P2, P3 and P4 are located on electrode E5, between E4 and E5, E4 and E1, respectively.

As illustrated in Figure 5, the sensitivity magnitude decreases with the increase in height of sensing chamber until 1.67 mm for both the dual- and single-plane miniature planar 3D ECT sensors. However, the sensitivity magnitude increases after 1.67 mm for the dual-plane miniature planar 3D ECT sensor but further decreases until a plateau is reached for the single-plane miniature planar 3D ECT sensor. The lack of sensitivity variation beyond 1.67 mm in single-plane miniature planar 3D ECT sensor resulted in the dead zone which cannot sense the presence of object. The addition of top electrode plane in the dual-plane miniature planar 3D ECT sensor introduces sensitivity variation in the top region of sensing chamber and overcomes the dead zone found in the single-plane miniature

Figure 5 Axial resolution analysis of dual- and single-plane miniature planar 3D ECT sensors

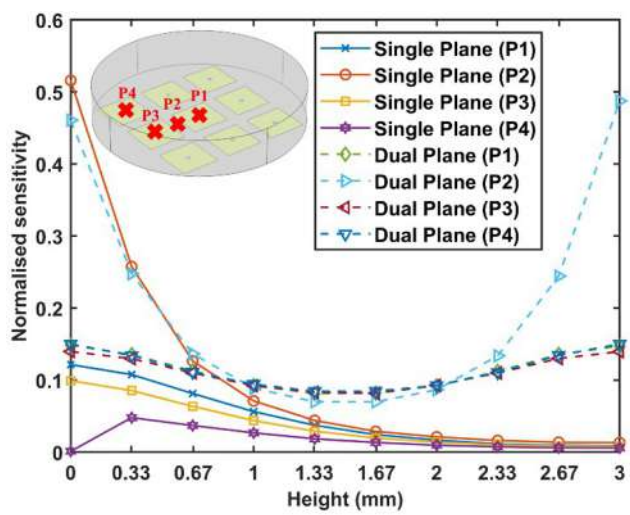

Source: Figure by authors

planar 3D ECT sensor. The presence of sensitivity variation at the top region of sensing chamber suggests that the height of object can be reconstructed accurately using the dual-plane miniature planar 3D ECT sensor because the samples are in region with full sensitivity coverage along vertical direction.

Fabrication of sensor and experimental setup

Fabrication of dual-plane miniature planar 3D electrical capacitance tomography sensor

The dual-plane miniature planar 3D ECT sensor was fabricated according to the dimension of the simulation model in Figure 1 for experimental investigation. Figure 6 shows the construction of dual-plane miniature planar 3D ECT sensor consisting of two 3×3 matrix electrode arrays, a top and a bottom electrode holder, a polydimethylsiloxane (PDMS) sensing chamber and a precision three-axis mechanical stage. The 3×3 matrix electrode array was fabricated onto printed circuit board (PCB) using standard manufacturing service provided by JLCPCB (JiaLiChuang [Hong Kong] Co., Limited). The surface of electrode array was coated with a thin layer of gold through the electroless nickel immersion gold process provided by the PCB manufacturer to prevent oxidation and wear on the electrodes. The thickness of the PCB is 1.6 mm. Because ECT is a non-invasive electrical tomography system, a thin PDMS film and a glass coverslip were used to insulate the top and bottom plane electrode surface from direct contact with the test samples. The combined thickness of the PDMS film and glass coverslip is 0.25 mm as measured using a digital vernier caliper (Mitutoyo CD-6″ CSX). The insulated electrode arrays were glued onto the top and bottom electrode plane holder as shown in Figure 6(b) and (c). The bottom electrode plane formed the single-plane miniature planar 3D ECT sensor that was used for 3D imaging performance comparison. Eventually, the top and bottom electrode planes were mounted onto the precision three-axis mechanical stage. A sensing chamber with a height of 3 mm was fabricated using PDMS and was inserted in between the top and bottom electrode planes.

Figure 7 shows the experimental set-up for the characterisation and 3D image reconstruction using dual-plane miniature planar 3D ECT sensor. The bottom electrode plane and the precision three-axis mechanical stage were mounted onto a 5 mm thick A4-sized Perspex sheet which function as a base for the sensor. The dual-plane miniature planar 3D ECT sensor was connected to the 18 channels of the data acquisition system (DAS) via coaxial cables (RG178 SMA-M to UFL) for measuring the interelectrode capacitance. Meanwhile, the DAS was connected to a host computer to perform the data collection and 3D image reconstruction. To perform 3D image reconstruction using single-plane miniature planar 3D ECT sensor, the top electrode plane and the precision three-axis mechanical stage were removed from the set-up.

Capacitance measurement characterisation

The dual-plane miniature planar 3D ECT sensor was characterised and compared to the single-plane miniature planar 3D ECT sensor based on the capacitance measurement. The capacitance signal was measured using a DAS developed in-house. The capacitance signal measured by the DAS is in terms of voltage. The interelectrode voltage of the developed sensor was measured for empty PDMS sensing chamber and PDMS sensing chamber filled with chicken meat sample. To provide a general idea of the performance of DAS, the average standard deviation of DAS was computed from 100 repetitive measurements of the 153 electrode pair combinations of dual plane on-chip 3D ECT sensor. The average standard deviation of DAS was computed to be 0.2656 mV. Meanwhile, the signal-to-noise ratio (SNR) of voltage measurement using the DAS ranges from 9.24 dB to 59.02 dB among the 153 electrode pair combinations.

Electrode plane separation and sensing height

The PDMS sensing chamber in this research was fabricated with a height of 3 mm based on the simulation model. This fixed the separation of the top and bottom electrode plane at

Figure 6 Development on dual-plane miniature planar 3D ECT sensor

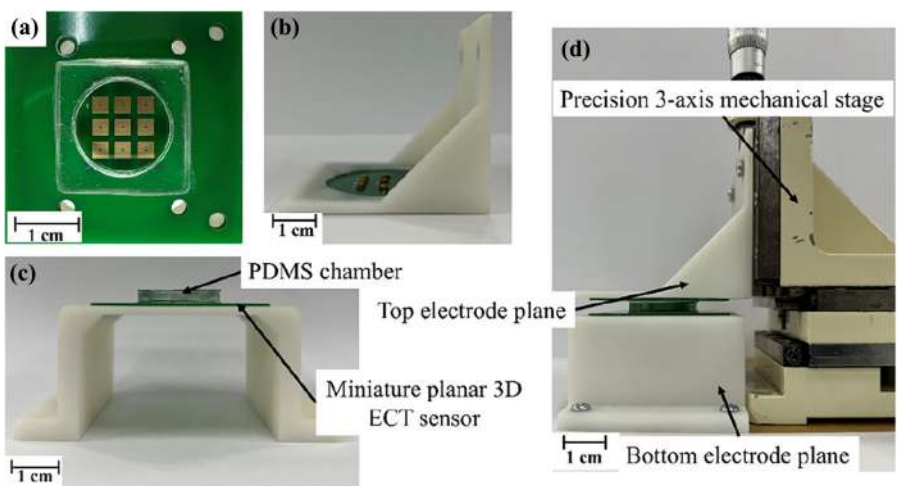

Notes: (a) Fabricated 3×3 matrix electrode array; (b) top electrode plane; (c) bottom electrode plane; (d) assembly of dual-plane miniature planar 3D ECT sensor
Source: Figure by authors

Figure 7 Experimental set-up for characterisation of dual-plane miniature planar 3D ECT sensor

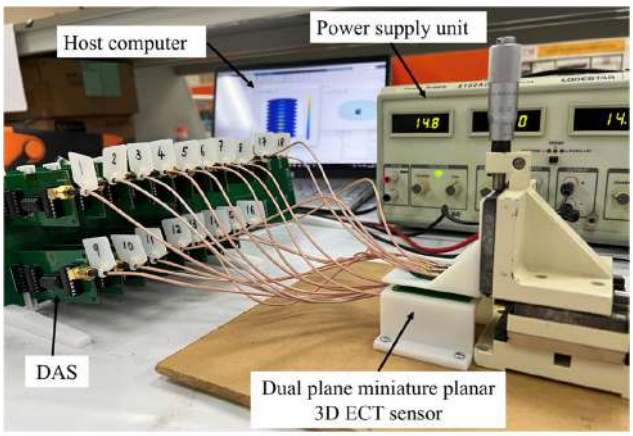

Source: Figure by authors

3 mm. Therefore, the electrode plane separation and the sensing height of dual-plane miniature planar 3D ECT sensor were characterised experimentally to confirm the practicality of the 3 mm electrode plane separation for real-world application. The electrode plane separation was characterised by measuring the voltage of parallel electrode pair such as between E1–E14, E1–E15, E1–E17 and E1–E18 at electrode plane separation of 1 to 10 mm with 1 mm step increment.

Meanwhile, the sensing height of dual-plane miniature planar 3D ECT sensor was evaluated based on the number of independent electrode pair voltage measurements available at different heights. In this experiment, a 2 mm thick 3D printed polylactic acid (PLA) block was suspended in between the top and bottom electrode planes. Its distance from both electrode planes was equal. The height between the PLA block and the electrode surfaces varied between 2 and 10 mm with 2 mm step increment. The measured voltage measurements are referenced against the empty sensor measurements. The measurements above two times the noise level of DAS of 0.2656 mV are considered as they contribute to image reconstruction. A higher number of independent measurements is desired, as it reflects the ability of the dual-plane miniature planar 3D ECT sensor to detect the presence of PLA block.

Experimental 3D image reconstruction

The 3D image reconstruction experiment was performed using the dual- and single-plane miniature planar 3D ECT sensors for comparison of the 3D imaging performance. In this experiment, a 2 mm chicken meat cube as shown in Figure 8 was used as the imaging sample, and the background medium was air. Prior to the imaging experiment, the dual- and single-plane miniature planar 3D ECT sensors were calibrated using the voltage of empty PDMS sensing chamber and PDMS sensing chamber filled with chicken meat sample. The 2 mm chicken meat cube sample was placed at test positions P1, P2, P3 and P4 as shown in Figure 5 for 3D image reconstruction. A 6 kHz excitation signal with an amplitude of 10 $V_{p\text{-}p}$ was supplied by the DAS for 3D imaging reconstruction.

Figure 8 Photograph of the 2 mm chicken meat cube used for 3D imaging experiments

Source: Figure by authors

The reconstructed 3D image was quantitatively evaluated using the correlation coefficient (CC). The formulation of CC is given by:

$$CC = \frac{\sum_{i=1}^{N}(\varepsilon_i - \overline{\varepsilon})(\hat{\varepsilon}_i - \overline{\hat{\varepsilon}})}{\sqrt{\sum_{i=1}^{N}(\varepsilon_i - \overline{\varepsilon})^2 \sum_{i=1}^{N}(\hat{\varepsilon}_i - \overline{\hat{\varepsilon}})^2}} \quad (5)$$

where ε and $\hat{\varepsilon}$ are the reconstructed permittivity distribution and true permittivity distribution, respectively. Meanwhile, $\overline{\varepsilon}$ and $\overline{\hat{\varepsilon}}$ are the means of ε and $\hat{\varepsilon}$. The CC computes the degree of similarity between the reconstructed image and the chicken meat cube sample. The $\hat{\varepsilon}$ is replaced by the simulated permittivity distribution using COMSOL Multiphysics.

Results and discussion

Capacitance measurement of sensor

Figure 9 compares the voltage measurement of dual- and single-plane miniature planar 3D ECT sensors when the PDMS sensing chamber is empty and filled with chicken meat sample. The voltage measurement of electrode pair combinations E1–E2 to E1–E18 was presented for a clear visualisation, as they include of all the measurement trend of the remaining electrode pair combinations. The electrode pair E1–E2 corresponds to the electrode pair 1 in Figure 9.

Figure 9 shows that the dual-plane miniature planar 3D ECT sensor produces additional electrode pair combinations between the bottom and top electrode plane such as E1–E10 to E1–E18 that are not found in single-plane miniature planar 3D ECT sensor. In addition, the electrode pair combinations E1–E15 and E1–E18 have higher voltage reading than the other top and bottom electrode pair combinations. This verifies the presence of sensitivity maps that extend from bottom to the top of sensing chamber in dual-plane miniature planar 3D ECT sensor as seen in Figure 3, as there are coupling between the top and bottom electrode pair combinations. As illustrated in Figure 9, the voltage measurement of empty and filled PDMS chamber of dual-plane miniature planar 3D ECT sensor is lower than single-plane miniature planar 3D ECT sensor. This is caused by the shielding effect introduced by the unused electrodes in either the top or bottom electrode plane. The unused electrodes for sensing are connected to virtual ground of the op-amp in capacitance

Figure 9 Voltage measurement of empty and filled PDMS chamber using dual- and single-plane miniature planar 3D ECT sensors

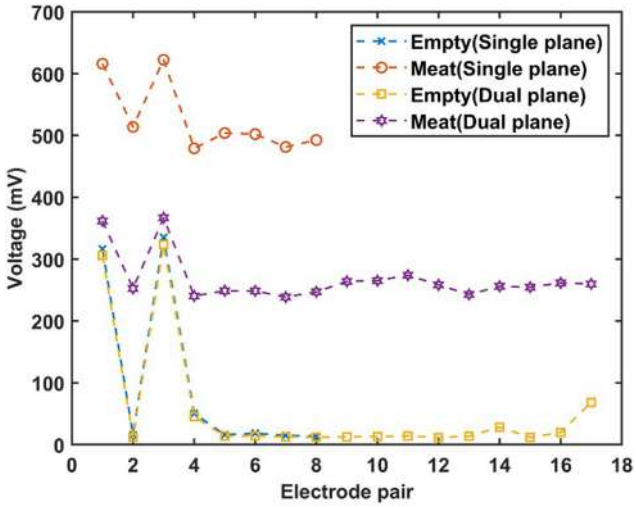

Source: Figure by authors

measurement circuit of DAS resulting in either the top or bottom electrode plane acting as a ground plane during the measurement cycle. The drop in voltage measurement does not affect the image reconstruction because the measured voltage is within the measurement range of the developed DAS.

Electrode plane separation and sensing height

Figure 10(a) shows the voltage measurement of the parallel electrode pair combinations for dual-plane miniature planar 3D ECT sensor in electrode plane separation experiment. The voltage of the parallel electrode pair combinations decreases as the electrode plane separation increases. This indicates that the coupling between the top and bottom electrode pair combination weakens with increase in electrode plane separation. The electrode pair combination E1–E18 has the highest voltage among the other electrode pair combinations because the electrodes are directly opposite to each other. The other parallel electrode pair combinations are able to produce voltage measurement although they are not directly opposite to each other. This indicates that coupling between the directly opposite and non-opposite parallel electrode pair combinations are present, and they contribute to the extended sensitivity map between the bottom and top of sensing chamber as shown in Figure 3. The limit of the electrode plane separation was identified based on electrode pair combination E1–E14 because it has the lowest voltage. The limit of electrode plane separation of dual-plane miniature planar 3D ECT sensor was found to be 8 mm, as a plateau was reached after 8 mm electrode plane separation.

Meanwhile, Figure 10(b) shows the number of independent measurements of dual-plane miniature planar 3D ECT sensor for sensing height experiment. The number of independent measurements decreases sightly when the height of PLA block increases from 2 to 3 mm. This indicates that the dual-plane miniature planar 3D ECT sensor can sense the presence of PLA block due to the sufficient coupling between the top and bottom electrode planes. Beyond the height of 3 mm, the number of independent measurements decreases drastically until a plateau is reached at a height of 8 mm, indicating the limit of sensing height. By varying the height of the PLA block from the electrode plane, the separation of top and bottom electrode plane also varies accordingly. For instance, when the PLA block was 2 and 3 mm above the bottom electrode plane, the separation of top and bottom electrode planes was 6 and 8 mm, respectively. This shows that at the 8 mm limit of electrode plane separation, the dual-plane miniature planar 3D ECT sensor can still produce a hundred of independent measurements for image reconstruction. Therefore, it was verified experimentally that the 3 mm electrode plane separation used in simulation study and the fabrication of PDMS sensing chamber height were practical and realistic, as it is within the 8 mm maximum limit of electrode plane separation.

3D image reconstruction of chicken meat cube sample

Figure 11 shows the placement and reconstructed 3D image of the 2 mm chicken meat cube sample in the PDMS sensing chamber at test positions P1, P2, P3 and P4. The reconstructed 3D image using dual- and single-plane miniature planar 3D

Figure 10 Plot of (a) measured voltage of parallel electrode pairs at different electrode plane separation and (b) number of independent measurements at different sensing height of dual-plane miniature planar 3D ECT sensor

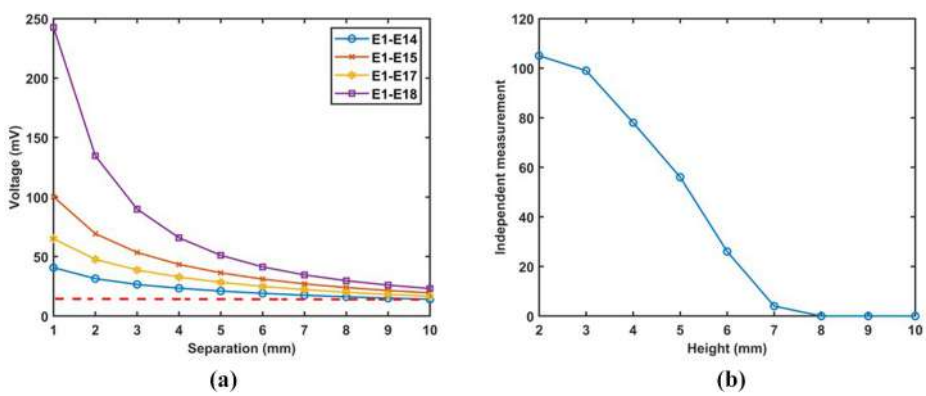

Source: Figure by authors

ECT sensors are visualised as the blue isosurface region. A 2 mm reference cube is superimposed onto the reconstructed 3D image which represent the actual position of the 2 mm chicken meat cube sample in the sensing chamber.

Figure 11 shows that the reconstructed 3D image by the dual-plane miniature planar 3D ECT sensor occupies the reference cube, while the 3D image reconstructed by single-plane miniature planar 3D ECT sensor occupies half the reference cube only. This indicates that the dual-plane miniature planar 3D ECT sensor is effective in reconstructing the height of test samples consistently at all the test positions. The improvement in 3D imaging performance of dual-plane miniature planar 3D ECT sensor is attributed to the addition of top electrode plane which extended the sensitivity distribution between the bottom and top electrode planes. The extended sensitivity distribution introduces variation in sensitivity along the vertical direction which allows the height of the sample to be reconstructed consistently throughout the different test positions in the PDMS sensing chamber. The extended sensitivity distribution was proven experimentally by the presence of voltage measurement, indicating the coupling between the top and bottom electrode pair combinations. Moreover, artefacts are reconstructed at test position P4 of single-plane miniature planar 3D ECT sensor but absent in dual-plane miniature planar 3D ECT sensor. This suggests that the 3D image reconstruction using the dual-plane miniature planar 3D ECT sensor is less affected by noise, and it is in accordance with the SVD analysis sensitivity map in Figure 4.

The quality of the reconstructed 3D images by the dual- and single-plane miniature planar 3D ECT sensor was evaluated quantitatively using CC as shown in Figure 12. The reconstructed 3D image of dual-plane miniature planar 3D ECT sensor has higher quality than the single-plane miniature planar 3D ECT sensor, which is indicated by the higher average CC of 0.6602 as compared to 0.5176 of respective sensors. This indicates that the reconstructed 3D image by dual-plane miniature planar 3D ECT sensor has high resemblance to the chicken meat cube sample. The 28% improvement in average CC of dual-plane miniature planar 3D ECT sensor is related to the improvement in height reconstruction using the dual-plane miniature planar 3D ECT sensor as shown in Figure 11. The highest CC is obtained at test position P1 of dual-plane miniature planar 3D ECT sensor. This is because it is surrounded by the most neighbouring and opposing electrode pair combinations that refined the vertical and horizontal resolutions of the reconstructed 3D image.

The 3×3 matrix electrode array proposed in this study highlights several benefits as compared to the electrode array design in literature. In terms of the number of electrodes, the proposed 3×3 matrix electrode array can be considered having an optimal number of electrodes. Ye *et al.* (2015) demonstrated that 3D image reconstructed using dual-plane sensor design can be reconstructed with a minimum of four electrodes arranged in 2×2 matrix on each electrode plane. However, this puts the image quality of the sensor by Ye *et al.* (2015) at a CC of 0.5 found at test position P4 when compared to the dual-plane sensor design in this work. A similar result can also be expected from the electrode array design of 2×3 matrix by Ren and Yang (2017). This is because the sensor design of Ye *et al.* (2015) and Ren and Yang (2017) resulted in two neighbouring and one opposing electrode pairs that contribute to image reconstruction only. With the 3×3 matrix electrode array design, the number of neighbouring and opposing electrode pairs was increased, which enable the sensor to achieve high

Figure 11 Experimental 3D image reconstruction of chicken meat cube sample using dual- and single-plane miniature planar 3D ECT sensors

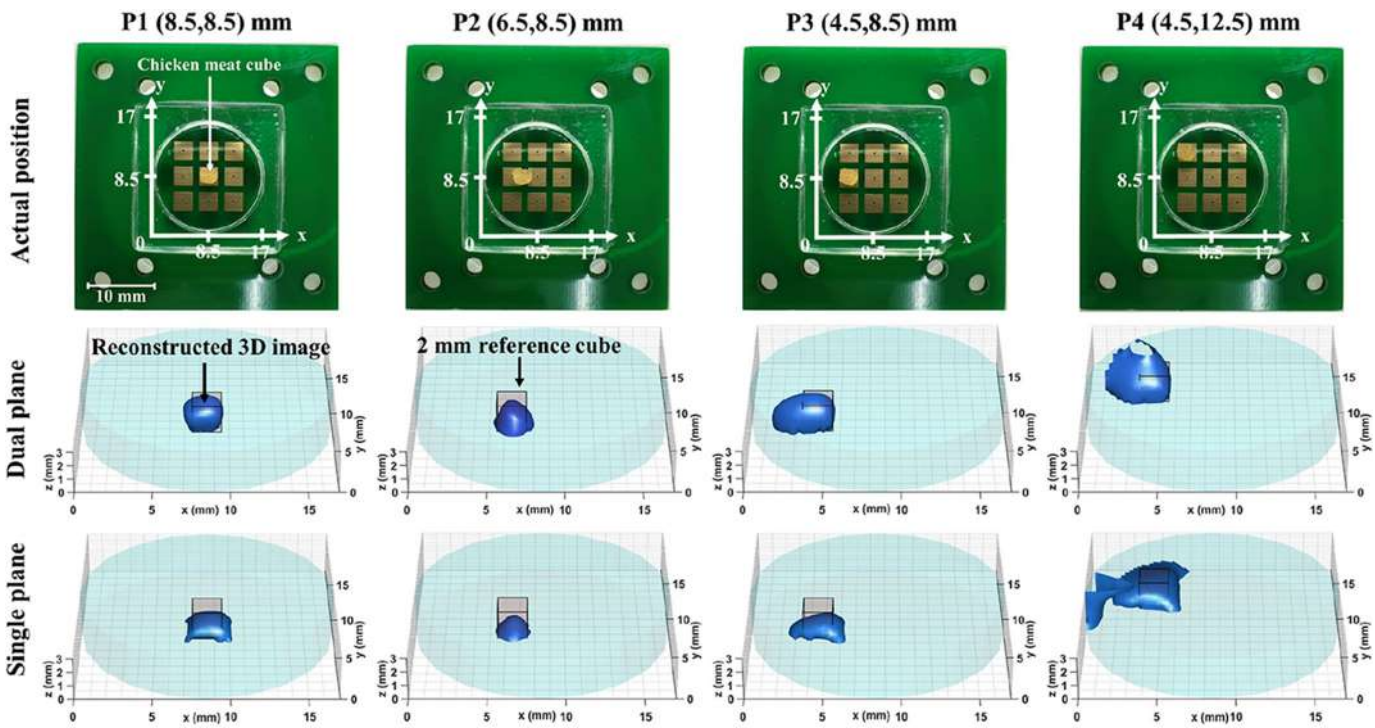

Source: Figure by authors

Figure 12 Correlation coefficient and average correlation coefficient of reconstructed 3D image at test positions P1, P2, P3 and P4

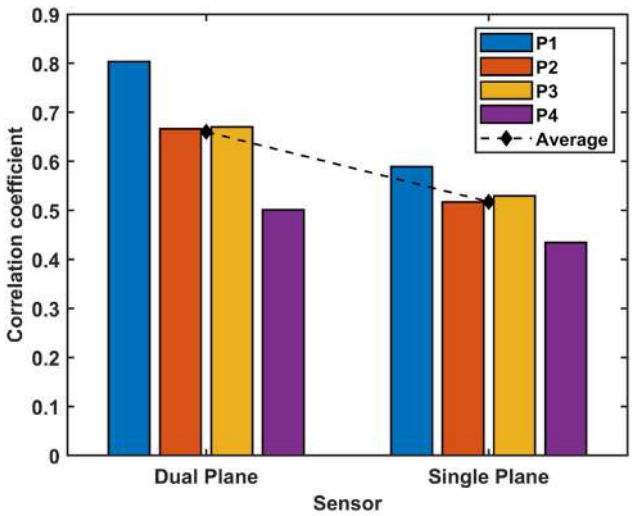

Source: Figure by authors

CC of reconstructed image such as at test positions P1, P2 and P3.

Besides, the 3×3 matrix electrode array dual-plane miniature planar 3D ECT sensor could improve the frame rate of capacitance measurement because 18 electrodes were used instead of 24 electrodes in Wei *et al.* (2015). The experiment results also revealed that the increase in number of electrodes due to the addition of electrode planes performed better in image reconstruction than the increase in number of electrodes within a single-electrode plane. This can be seen in the improved height reconstruction of the dual-plane miniature planar 3D ECT sensor as compared to the 4×4 matrix array single-plane planar ECT sensor in Figure 2. In addition, the 3×3 matrix electrode array dual-plane miniature planar 3D ECT sensor reconstructed 3D image with consistent quality at different test positions as compared to the varying image quality in dual-plane peripheral electrode array sensor of Hor *et al.* (2023). This is because the sensitive region of 3×3 matrix electrode array dual-plane miniature planar 3D ECT sensor covers the entire sensing region, while the sensitive region of sensor in Hor *et al.* (2023) mainly concentrates the circumference of sensing chamber only.

Conclusion

In this paper, a dual-plane miniature planar 3D ECT sensor consisting of two electrode planes made of 3×3 matrix electrode array was developed and investigated. The 3×3 matrix electrode array design optimises the electrode pair combinations to neighbouring and opposing electrode pair combinations that have high contribution in image reconstruction. A series of simulation studies were performed on the sensitivity map of the dual-plane miniature planar 3D ECT sensor, and it was compared to a single-plane miniature planar 3D ECT sensor. The simulation results revealed that extended sensitivity distribution from the bottom to the top electrode plane was present in the dual-plane miniature planar 3D ECT sensor. This was attributed to the sensitivity maps generated from the top and bottom electrode pairs. The SVD analysis showed that the dual-plane miniature planar 3D ECT sensor is less ill-posed than single-plane miniature planar 3D ECT sensor in 3D image reconstruction. In addition, the axial resolution analysis of the sensitivity map demonstrated that sensitivity variation can be found throughout the sensing region indicating improved height sensing of the dual-plane miniature planar 3D ECT sensor as compared to single-plane miniature planar 3D ECT sensor. In general, the simulation results indicated that the dual-plane miniature planar 3D ECT sensor could outperform the single-plane miniature planar 3D ECT sensor in terms of 3D image reconstruction and height reconstruction.

The dual-plane miniature planar 3D ECT sensor was fabricated for experimental characterisation and 3D image reconstruction. It was characterised in terms of the electrode plane separation and the sensing height. Experimental characterisation results revealed that the optimal electrode plane separation of the dual-plane miniature planar 3D ECT sensor is 3 mm. At 3 mm electrode plane separation, it can produce high number of independent measurements which are necessary in reconstructing high-quality 3D image. One drawback of the dual-plane miniature planar 3D ECT sensor is that the measured voltage for empty and filled PDMS sensing chamber is lower than the single-plane miniature planar 3D ECT sensor due to the grounding effect imposed by the unused electrodes from either the top or bottom electrode during the electrode pair measurement sequence.

The 3D image reconstruction was performed using a 2 mm chicken meat cube sample at the test positions using the dual- and single-plane miniature planar 3D ECT sensors for comparison. The dual-plane miniature planar 3D ECT sensor improved the quality of reconstructed 3D image by 28% as compared to the single-plane miniature planar 3D ECT sensor. This indicates that the dual-plane miniature planar 3D ECT sensor miniature planar 3D ECT sensor miniature planar 3D ECT sensor has better 3D image and height reconstruction performance as compared to single-plane miniature planar 3D ECT sensor. The demonstrated capability of the dual-plane miniature planar 3D ECT sensor would benefit application such as monitoring of 3D cultured cells in lab-on-chip platform. Specifically, the miniature size of dual-plane miniature planar 3D ECT sensor would ease the integration onto lab-on-chip platform and provide instant non-destructive monitoring of the approximate distribution and height of samples.

References

Hor, X.F., Leow, P.L., Ali, M.S.M., Chee, P.S., Din, S.M. and Gooi, W.P. (2023), "Electrode configuration study for three-dimensional imaging of on-chip ECT", *Engineering Research Express*, Vol. 5 No. 2, doi: 10.1088/2631-8695/acc513.

Huang, K., Meng, S., Guo, Q., Yang, W., Zhang, T., Ye, M. and Liu, Z. (2019), "Effect of electrode length of an electrical capacitance tomography sensor on gas–solid fluidized bed measurements", *Industrial & Engineering Chemistry Research*, Vol. 58 No. 47, pp. 21827-21841, doi: 10.1021/acs.iecr.9b03988.

Ma, G. and Soleimani, M. (2020), "A versatile 4D capacitive imaging array: a touchless skin and an obstacle-avoidance sensor for robotic applications", *Scientific Reports*, Vol. 10 No. 1, pp. 1-9, doi: 10.1038/s41598-020-68432-1.

Pan, Z., Wang, S., Li, P., Zhang, Y. and Wen, Y. (2021), "An optimization method of planar array capacitance imaging", *Sensors and Actuators A: Physical*, Vol. 327, p. 112724, doi: 10.1016/j.sna.2021.112724.

Porzuczek, J. (2014), "Applications of electrical capacitance tomography for research on phenomena occurring in the fluidised bed reactors", *Chemical and Process Engineering*, Vol. 35 No. 4, pp. 397-408, doi: 10.2478/cpe-2014-0030.

Ren, Z. and Yang, W. (2015), "A miniature two-plate electrical capacitance tomography sensor", *IEEE Sensors Journal*, Vol. 15 No. 5, pp. 3037-3049, doi: 10.1109/JSEN.2014.2383491.

Ren, Z. and Yang, W.Q. (2017), "Visualisation of tooth surface by electrical capacitance tomography", *Biomedical Physics & Engineering Express*, Vol. 3 No. 1, p. 015021, doi: 10.1088/2057-1976/3/1/015021.

Rodriguez-Frias, M.A. and Yang, W. (2020), "Dual-modality 4-terminal electrical capacitance and resistance tomography for multiphase flow monitoring", *IEEE Sensors Journal*, Vol. 20 No. 6, pp. 3217-3225, doi: 10.1109/JSEN.2019.2955399.

Shen, J., Meng, S., Yang, W. and Ye, M. (2021), "Excitation strategies for 3-D electrical capacitance tomography sensors", *IEEE Transactions on Instrumentation and Measurement*, Vol. 70, doi: 10.1109/TIM.2021.3075038.

Suo, P., Sun, J., Tian, W., Sun, S. and Xu, L. (2021), "3-D image reconstruction in planar array ECT by combining depth estimation and sparse representation", *IEEE Transactions on Instrumentation and Measurement*, Vol. 70, doi: 10.1109/TIM.2021.3086903.

Tholin-Chittenden, C. and Soleimani, M. (2017), "Planar array capacitive imaging sensor design optimization", *IEEE Sensors Journal*, Vol. 17 No. 24, pp. 8059-8071, doi: 10.1109/JSEN.2017.2719579.

Tholin-Chittenden, C., Abascal, J.F.P.J. and Soleimani, M. (2018), "Automatic parameter selection of image reconstruction algorithms for planar array capacitive imaging", *IEEE Sensors Journal*, Vol. 18 No. 15, pp. 6263-6272, doi: 10.1109/JSEN.2018.2844549.

Wang, H. and Yang, W. (2021), "Application of electrical capacitance tomography in pharmaceutical fluidised beds – a review", *Chemical Engineering Science*, Vol. 231 No. 40, p. 116236, doi: 10.1016/j.ces.2020.116236.

Wei, H.Y., Qiu, C.H. and Soleimani, M. (2015), "Evaluation of planar 3D electrical capacitance tomography: from single-plane to dual-plane configuration", *Measurement Science and Technology*, Vol. 26 No. 6, p. 65401, doi: 10.1088/0957-0233/26/6/065401.

Wen, Y., Zhang, Z., Zhang, Y. and Sun, D. (2017), "Redundancy analysis of capacitance data of a coplanar electrode array for fast and stable imaging processing", *Sensors*, Vol. 18 No. 2, p. 31, doi: 10.3390/s18010031.

Yang, Y., Jia, J., Smith, S., Jamil, N., Gamal, W. and Bagnaninchi, P.O. (2017), "A miniature electrical impedance tomography sensor and 3-D image reconstruction for cell imaging", *IEEE Sensors Journal*, Vol. 17 No. 2, pp. 514-523, doi: 10.1109/JSEN.2016.2631263.

Yao, J. and Takei, M. (2017), "Application of process tomography to multiphase flow measurement in industrial and biomedical fields: a review", *IEEE Sensors Journal*, Vol. 17 No. 24, pp. 8196-8205, doi: 10.1109/JSEN.2017.2682929.

Ye, J., Yang, W. and Wang, C. (2020), "Investigation of spatial resolution of electrical capacitance tomography based on coupling simulation", *IEEE Transactions on Instrumentation and Measurement*, Vol. 69 No. 11, pp. 8919-8929, doi: 10.1109/TIM.2020.3001461.

Ye, Z., Wei, H.Y. and Soleimani, M. (2015), "Resolution analysis using fully 3D electrical capacitive tomography", *Measurement*, Vol. 61, pp. 270-279, doi: 10.1016/j.measurement.2014.10.060.

Zhang, Y., Sun, Y. and Wen, Y. (2021), "An imaging algorithm of planar array capacitance sensor for defect detection", *Measurement*, Vol. 168, p. 108466, doi: 10.1016/j.measurement.2020.108466.

Corresponding author

Pei Ling Leow can be contacted at: leowpl@utm.my